JCTC Journal of Chemical Theory and Computation

Article

Cite This: J. Chem. Theory Comput. 2018, 14, 4640−4650

pubs.acs.org/JCTC

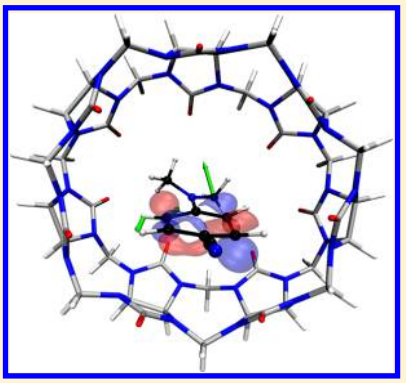
Analytic Excited State Gradients for the QM/MM Polarizable Embedded Second-Order Algebraic Diagrammatic Construction for the Polarization Propagator PE-ADC(2)

Alireza Marefat Khah,* Sarah Karbalaei Khani, and Christof Hättig

Arbeitsgruppe Quantenchemie, Ruhr-Universität Bochum, Bochum D-44801, Germany

Supporting Information

ABSTRACT: An implementation of a QM/MM embedding in a polarizable environment is presented for second-order Møller−Plesset perturbation theory, MP2, for ground state energies and molecular gradients and for the second-order Algebraic Diagrammatic Construction, ADC(2), for excitation energies and excited state molecular gradients. In this implementation of PE-MP2 and PE-ADC(2), the polarizable embedded Hartree−Fock wave function is used as uncorrelated reference state. The polarization-correlation cross terms for the ground and excited states are included in this model via an approximate coupling density. A Lagrangian formulation is used to derive the relaxed electron densities and molecular gradients. The resolution-of-the-identity approximation speeds up the calculation of four-index electron repulsion integrals in the molecular orbital basis. As a first application, the method is used to study the photophysical properties of host−guest complexes where the accuracy and weaknesses of the model are also critically examined. It is demonstrated that the ground state geometries of the full quantum mechanical calculation for the supermolecule can be well reproduced. For excited state geometries, the deviations from the supermolecular calculation are slightly larger, but still the environment effects are captured qualitatively correctly, and energy gaps between the ground and excited states are obtained with sufficient accuracy.



Downloaded via BOCHUM LIBRARIES on December 22, 2018 at 13:44:48 (UTC).
See https://pubs.acs.org/sharingguidelines for options on how to legitimately share published articles.

INTRODUCTION

Most photochemistry happens in solution, on surfaces, or in biomolecular matrices where the inhomogeneous structure of the molecular environment can disturb the electronic and molecular structure of the chromophore and thereby have non-negligible effects on various molecular properties.[1] This leads to a demand for multiscale methods that can be applied to systems with many atoms but only treat an active site, which has much fewer atoms, with high accuracy, so that the computational costs are still manageable. Often specific interactions between the system of interest and the environment are significant and require that the atomistic structure of the environment is explicitly taken into account. For these systems, an efficient way to include the effects of a complex molecular environment in a quantum chemical calculation is to use QM/MM methods,[2,3] which describe the environment at an atomistic level using classical mechanics and electrostatics.

In the QM/MM approach, the energy of the total system can be divided into the energies of the QM and the MM subsystems and an interaction term, $E^{\mathrm{QM/MM}} = E^{\mathrm{QM}} + E^{\mathrm{MM}} + E^{\mathrm{QM\text{-}MM}}$. The interaction between the QM and MM subsystems is often approximated by mechanical contributions (which do not affect the electrons) plus an electrostatic interaction between the electronic density of the QM subsystem with a set of point charges and also static multipole moments (dipoles, quadrupoles, etc.). In such an electrostatic multipole embedding, the MM subsystem shows no direct response to the changes in the electronic density of the QM subsystem that happen at the time scale of electronic excitations. It can only respond indirectly through changes in the structure, which happen at much slower time scales. Therefore, a polarizable embedding is important for a realistic description of environment effects on electronic excitation processes.[4]

The QM/MM approach has been used for a long time with several QM methods for ground state energies and structures where (nonpolarizable) electrostatic multipole interactions are often sufficient. But when it comes to electronic excitations and excited state structures for which the inclusion of the polarizability of the environments is essential, the QM/MM approach has only rarely been used with wave-function-based methods that go beyond the time-dependent density functional theory (TDDFT).

In recent years, the QM/MM polarizable embedding method has been developed to describe different excited state properties[5,6] in combination with TDDFT[7] and coupled cluster wave functions[8−10] as well as multireference methods.[11,12] Implementations for analytic molecular gradients for polarizable MM embeddings have been reported for ground state structures at the DFT[13,14] and MP2[15] levels and for excited states at the TDDFT level.[16,17]

The correct description of charge-transfer states with TDDFT is already problematic in the gas phase. If the

Received: April 25, 2018
Published: July 24, 2018

© 2018 American Chemical Society

DOI: 10.1021/acs.jctc.8b00396
J. Chem. Theory Comput. 2018, 14, 4640−4650

quantum system is placed in a polarizable environment even functionals that were designed for electronic excitations like CAM-B3LYP[18] can fail for systems with charge transfer states.[19] Since wave-function-based methods do not suffer from this problem, the second-order methods CC2[20] and ADC(2)[21] are often the methods of choice for medium-sized quantum systems where they have only moderately higher computational cost.[22−24] For the calculation of molecular gradients for excited-state potential energy surfaces, ADC(2) is of particular interest as for this method the computational costs for the gradients are up to a factor of 4 lower than those for CC2, while the accuracy of the resulting structures is almost the same for both methods.[25] Furthermore, ADC(2) has a Hermitian secular matrix, which provides, in contrast to CC2, a physically correct description of the potential energy surface in the vicinity of conical intersection.[22,26]

In the current contribution, we report for PE-ADC(2) the first implementation of analytic excited state gradients for a correlated wave-function-based method in an atomistic polarizable embedding. Applications of the PE-ADC(2) gradients are presented for host−guest systems where supermolecular reference calculations are still possible so that they can be used to evaluate and discuss the strengths and also weaknesses of the approach.

THEORY

Polarizable Embedded Hartree−Fock. For the sake of briefness, we will only recapitulate the essential equations for the theory of the polarizable embedding.[5,7] For a more detailed discussion of the physical background of polarizable embeddings and the definition and implementation of linear response theory in a polarizable embedding, we refer the reader to a recent review by List et al.[27] We start with the free energy expression of the polarizable embedded Hartree−Fock (PE-HF) model:

$$\begin{aligned}\mathcal{G}^{\mathrm{PE-HF}} &= \langle \mathrm{HF}|\hat{H}^{\mathrm{QM}} + \hat{G}^{\mathrm{es}}|\mathrm{HF}\rangle \\ &\quad - \frac{1}{2}\sum_{uv}(F_u^{\mathrm{ne}} + F_u^{\mathrm{elec}}(\mathbf{D}^{\mathrm{HF}})) \\ &\quad \times R_{uv}(F_v^{\mathrm{ne}} + F_v^{\mathrm{elec}}(\mathbf{D}^{\mathrm{HF}})) + E^{\mathrm{ne}}\end{aligned} \tag{1}$$

In this equation, $\hat{H}^{\mathrm{QM}}$ is the vacuum-like Hamiltonian for the QM system. The interaction of the QM electrons with the static multipole moments of the MM system are taken into account through the one-electron operator:

$$\hat{G}^{\mathrm{es}} = \sum_u Q_u^{\mathrm{es}} \sum_{pq} \varepsilon_{pq}^u \hat{E}_{pq} \tag{2}$$

where Q_u^{es} and ε_{pq}^u are, respectively, the static (permanent) multipole moments and the multipole interaction integrals. The index u runs here over all multipole components at all MM sites. Finally, $\hat{E}_{pq}$ is the second quantization singlet replacement operator.[28] Here and in the following, the indices p, q, r, and s are used for general molecular orbitals. R_{uv} is the response matrix with the indices u and v running in general over all components of induced multipole moments at polarizable MM sites. In the current work, we only include distributed dipole−dipole polarizabilities. F_v^{ne} are then the components of the electric fields at the polarizable MM sites due to the nuclei in the QM subsystem and the static multipoles of all other MM sites, and $F_v^{\mathrm{elec}}(\mathbf{D})$ are the contributions due to electron density $\mathbf{D}$. For further details, we refer to ref 7. The last term in eq 1 contains the nonelectronic contributions to the free energy:

$$E^{\mathrm{ne}} = E^{\mathrm{nuc\text{-}es}} + E^{\mathrm{MM}} + E_{6\text{-}12}^{\mathrm{LJ}} \tag{3}$$

where $E^{\mathrm{nuc\text{-}es}}$ is the electrostatic interaction of the QM nuclei with the MM sites, and E^{MM} is the internal energy of the MM system. To account for the London dispersion interaction and the short-range repulsion, we include a Lennard-Jones 6-12 term ($E_{6\text{-}12}^{\mathrm{LJ}}$) between the atoms in the QM and the atoms in the MM subsystem,

$$E_{6\text{-}12}^{\mathrm{LJ}} = \sum_{s=1}^{S}\sum_{m\in\mathrm{QM}} \epsilon^{sm}\left[\left(\frac{r_{sm}}{|\mathbf{R}_m - \mathbf{R}_s|}\right)^{12} - 2\left(\frac{r_{sm}}{|\mathbf{R}_m - \mathbf{R}_s|}\right)^{6}\right] \tag{4}$$

The pair interaction parameters r_{sm} and ϵ^{sm} are derived from atomic parameters using the Lorentz−Berthelot combination rules $r_{sm} = \frac{1}{2}(r_s + r_m)$ and $\epsilon^{sm} = \sqrt{\epsilon^s \epsilon^m}$ where r_s and ϵ^s are, respectively, atomic radii and well depths.

The minimization of the free energy for the polarizable embedded Hartree−Fock model, $\mathcal{G}^{\mathrm{PE\text{-}HF}}$, with respect to variations of the orbitals leads to the condition

$$\langle \mathrm{HF}|[\hat{H}^{\mathrm{QM}} + \hat{G}^{\mathrm{es}} + \hat{G}^{\mathrm{pol,HF}}, \hat{E}_{pq}^{-}]|\mathrm{HF}\rangle = 0 \tag{5}$$

where we introduced the antisymmetrized operators $\hat{E}_{pq}^{-} = \hat{E}_{pq} - \hat{E}_{qp}$. The polarization contribution to the reaction field potential is given by

$$\begin{aligned}\hat{G}^{\mathrm{pol,HF}} &= -\sum_{uv}(F_v^{\mathrm{ne}} + F_v^{\mathrm{elec}}(\mathbf{D}^{\mathrm{HF}}))R_{vu}\sum_{pq}\varepsilon_{pq}^u \hat{E}_{pq} \\ &= \sum_u Q_u^{\mathrm{ind,HF}} \sum_{pq}\varepsilon_{pq}^u \hat{E}_{pq}\end{aligned} \tag{6}$$

Since within the PE model the interaction with the environment only affects the electrostatic potential experienced by the electrons and the nonelectronic contributions, its formulation and implementation for Kohn−Sham density functional theory (DFT) are analogous to the above equations. Working expression for analytic nuclear gradients at the PE-DFT and PE-HF level have been reported by List et al. in ref 13 and for conciseness will not be repeated here. As a part of the current work, we have implemented the gradients for PE-HF and PE-DFT in the HF and DFT gradient programs `grad` and `rdgrad` of a development version of the TURBOMOLE package.[29] The self-consistently optimized PE-HF determinant is used as reference wave function for the correlation treatment at the PE-MP2 and the calculation of excitation energies at the PE-ADC(2) level in accordance with the recent implementation of PERI-CC2 for excitation energies and one- and two-photon transition moments.[9,30]

Polarizable Embedded Second-Order Møller−Plesset Perturbation Theory. The reaction field scheme that has been used in previous work on PERI-CC2 reduces at the level of MP2, that is, when the CC2 cluster amplitudes are replaced by those from first-order perturbation theory, to a scheme that in the literature is known[31] as perturbation on the energy (PTE). The PTE scheme is also the reaction field scheme that is most consistent with second-order Møller−Plesset perturbation theory.[32] Within this scheme, the PE-MP2 correlation energy is calculated fully analogously to the vacuum case just using the molecular orbitals and the Fock operator

DOI: 10.1021/acs.jctc.8b00396
J. Chem. Theory Comput. 2018, 14, 4640−4650

$$\hat{F}^{\mathrm{PE}} = \hat{F}^{\mathrm{QM}} + \hat{G}^{\mathrm{HF}} \tag{7}$$

from a PE-HF calculation where $\hat{G}^{\mathrm{HF}} = \hat{G}^{\mathrm{es}} + \hat{G}^{\mathrm{pol,HF}}$. The working expressions for the PE-MP2 molecular gradients can be obtained by differentiating the orbital relaxed Lagrangian:

$$\begin{aligned} L^{\text{PE-MP2}} = {} & \langle \mathrm{HF}|\hat{H}^{\mathrm{QM}} + \hat{G}^{\mathrm{es}} + [\hat{W}^{\mathrm{QM}}, \hat{T}_2^{(1)}]|\mathrm{HF}\rangle \\ & + \langle \bar{t}_2^{(1)}|[\hat{F}^{\mathrm{PE}}, \hat{T}_2^{(1)}] + \hat{W}^{\mathrm{QM}}|\mathrm{HF}\rangle \\ & + \langle \mathrm{HF}|[\hat{H}^{\mathrm{QM}} + \hat{G}^{\mathrm{HF}}, \hat{\bar{\kappa}}]|\mathrm{HF}\rangle \\ & - \frac{1}{2}\sum_{uv}(F_u^{\mathrm{ne}} + F_u^{\mathrm{elec}}(\mathbf{D}^{\mathrm{HF}})) \\ & \times R_{uv}(F^{\mathrm{ne}} + F^{\mathrm{elec}}(\mathbf{D}^{\mathrm{HF}})) + E^{\mathrm{ne}} \end{aligned} \tag{8}$$

In the above equation, $\hat{T}_2^{(1)} = \sum_{\mu_2} t_{\mu_2}^{(1)} \tau_{\mu_2}$ is the double excitation operator built from the first-order amplitudes, $t_{\mu_2}^{(1)}$, with μ_2 running over all double replacements and $\langle \bar{t}_2^{(1)}| = \sum_{\mu_2} \bar{t}_{\mu_2}^{(1)} \langle \mu|$ is the first-order wave function correction built from the first-order Lagrange multipliers. $\hat{W}^{\mathrm{QM}}$ denotes the fluctuation potential operator and $\hat{\bar{\kappa}}$ is an operator that contains the orbital rotation Lagrange multipliers:

$$\hat{\bar{\kappa}} = \sum_{pq} \bar{\kappa}_{pq} \hat{E}_{pq}^{-} \tag{9}$$

The values of the orbital-rotation Lagrange multipliers $\bar{\kappa}_{pq}$ are determined by the CPHF (also known as Z-vector) equations, which are obtained by requiring $L^{\text{PE-MP2}}$ to be stationary with respect to orbital variations:

$$\sum_{rs} (\langle \mathrm{HF}|[[\hat{F}^{\mathrm{PE}}, \hat{E}_{pq}^{-}], \hat{E}_{rs}^{-}]|\mathrm{HF}\rangle + A_{pq,\mathrm{rs}}^{\kappa})\bar{\kappa}_{rs} = -\eta_{pq}^{\kappa,\mathrm{MP2}} \tag{10}$$

The right-hand-side vector η_{pq}^{κ} is given by

$$\begin{aligned} \eta_{pq}^{\kappa,\mathrm{MP2}} = {} & \langle \mathrm{HF}|[\hat{F}^{\mathrm{PE}} + \hat{W}^{\mathrm{QM}}, \hat{E}_{pq}^{-}] + [[\hat{W}^{\mathrm{QM}}, \hat{E}_{pq}^{-}], \hat{T}_2^{(1)}]|\mathrm{HF}\rangle \\ & + \langle \bar{t}_2^{(1)}|[[\hat{F}^{\mathrm{PE}}, \hat{E}_{pq}^{-}], \hat{T}_2^{(1)}] + [\hat{W}^{\mathrm{QM}}, \hat{E}_{pq}^{-}]|\mathrm{HF}\rangle \\ & + \langle \bar{t}_2^{(1)}|\left[\left(\frac{d\hat{F}^{\mathrm{PE}}}{d\kappa_{pq}} - [\hat{F}^{\mathrm{PE}}, \hat{E}_{pq}^{-}]\right), \hat{T}_2^{(1)}\right]|\mathrm{HF}\rangle \end{aligned} \tag{11}$$

and, thus, includes environment contributions only via $\hat{F}^{\mathrm{PE}}$ and the orbitals. The CPHF matrix $A_{pq,rs}^{\kappa}$ for the PE model is defined as

$$\begin{aligned} A_{pq,\mathrm{rs}}^{\kappa} = {} & \langle \mathrm{HF}|[[\hat{W}^{\mathrm{QM}}, \hat{E}_{pq}^{-}], \hat{E}_{rs}^{-}]|\mathrm{HF}\rangle \\ & + \sum_{uv} \langle \mathrm{HF}|[\hat{\varepsilon}^{u}, \hat{E}_{pq}^{-}]|\mathrm{HF}\rangle R_{uv} \langle \mathrm{HF}|[\hat{\varepsilon}^{v}, \hat{E}_{rs}^{-}]|\mathrm{HF}\rangle \end{aligned} \tag{12}$$

After solving the CPHF eqs 10, the effective one-electron density for MP2 can be calculated as in the vacuum case:[33,34]

$$D_{pq}^{\mathrm{eff}} = D_{pq}^{\mathrm{HF}} + \langle \bar{t}_2^{(1)}|[\hat{E}_{pq}, \hat{T}_2^{(1)}]|\mathrm{HF}\rangle + \frac{1}{2}(\bar{\kappa}_{pq} + \bar{\kappa}_{qp}) \tag{13}$$

For the derivation of the expressions for the PE-MP2 gradients, we split the PE-MP2 Lagrangian into $L^{\text{PE-MP2}} = L^{\mathrm{MP2,QM}} + \Delta L^{\mathrm{PE}}$ where $L^{\mathrm{MP2,QM}}$ contains the vacuum-like contributions and ΔL^{PE} the explicit PE terms, which are not present in the vacuum case:

$$\begin{aligned} \Delta L^{\mathrm{PE}} = {} & \langle \mathrm{HF}|\hat{G}^{\mathrm{es}}|\mathrm{HF}\rangle + \langle \bar{t}_2^{(1)}|[\hat{G}^{\mathrm{HF}}, \hat{T}_2^{(1)}]|\mathrm{HF}\rangle \\ & + \langle \mathrm{HF}|[\hat{G}^{\mathrm{HF}}, \hat{\bar{\kappa}}]|\mathrm{HF}\rangle \\ & - \frac{1}{2}\sum_{uv}(F_u^{\mathrm{ne}} + F_u^{\mathrm{elec}}(\mathbf{D}^{\mathrm{HF}})) \\ & \times R_{uv}(F_v^{\mathrm{ne}} + F_v^{\mathrm{elec}}(\mathbf{D}^{\mathrm{HF}})) + E^{\mathrm{ne}} \end{aligned} \tag{14}$$

$$\begin{aligned} = {} & -\frac{1}{2}\sum_{uv}(F_u^{\mathrm{ne}} + 2F_u^{\mathrm{elec}}(\mathbf{D}^{\mathrm{eff}}) - F_u^{\mathrm{elec}}(\mathbf{D}^{\mathrm{HF}})) \\ & \times R_{uv}(F_v^{\mathrm{ne}} + F_v^{\mathrm{elec}}(\mathbf{D}^{\mathrm{HF}})) \\ & + \sum_{pq} D_{pq}^{\mathrm{eff}} \sum_{u} Q_u^{\mathrm{es}} \varepsilon_{pq}^{u} + E^{\mathrm{ne}} \end{aligned} \tag{15}$$

The explicit embedding contributions to the gradients for the QM atoms are computed as

$$\begin{aligned} \frac{\mathrm{d}\Delta L^{\mathrm{PE}}}{\mathrm{d}x} = {} & \sum_{pq} D_{pq}^{\mathrm{eff}} \sum_{u} Q_u^{\mathrm{HF}} \frac{\mathrm{d}\varepsilon_{pq}^{u}}{\mathrm{d}x} + \sum_{pq} D_{pq}^{\mathrm{HF}} \\ & \times \sum_{u} (Q_u^{\mathrm{eff}} - Q_u^{\mathrm{HF}}) \frac{\mathrm{d}\varepsilon_{pq}^{u}}{\mathrm{d}x} + \sum_{u} Q_u^{\mathrm{eff}} \frac{\mathrm{d}\varepsilon_{\mathrm{nuc}}^{u}}{\mathrm{d}x} \\ & + \frac{\mathrm{d}E^{\mathrm{LJ}}}{\mathrm{d}x} \end{aligned} \tag{16}$$

The multipole moments Q_u^{eff} are the sum of the static and the induced moments computed from the MP2 density $\mathbf{D}^{\mathrm{eff}}$ and Q_u^{HF} are the respective Hartree−Fock counterparts. $\varepsilon_{\mathrm{nuc}}^{u}$ is the sum of the multipole-charge interaction tensors for the interaction with the nuclei, contracted with the nuclear charges.

The PE-MP2 model has been implemented for energies and molecular gradients in the `ricc2` program of a development version of the TURBOMOLE package.[29] The MPI-parallel implementation of the MP2 energy and gradients for the vacuum case have been described in ref 34. The contributions from $L^{\mathrm{MP2,QM}}$ to the molecular gradients are evaluated as described in the latter reference. We stress that our implementation of PE-MP2 uses, as the vacuum implementation, the resolution-of-the-identity (RI) approximation for the electron repulsion integrals and is parallelized with OpenMP and MPI, which makes it applicable to relatively large molecular systems.

PE-ADC(2) for Excited States Energy and Gradients. Although the underlying physical background of ADC(2) and CC2 are different, the kernel of the following discussion lies in the mathematical similarity between these methods, which facilitates easy development and implementation of the equations for PE-ADC(2) excitation energies and gradients as a simplification of PE-CC2.[22] In the framework of response theory,[35] excitation energies are obtained for nonvariational methods like CC2 as eigenvalues of the Jacobi matrix $\mathbf{A}$:

$$(\mathbf{A} - \omega^{f}\mathbf{1})\mathbf{E}^{f} = 0 \tag{17}$$

The CC2 Jacobian includes terms that only contribute in third or higher order to the excitation energies. These terms can be excluded by replacing in the CC2 Jacobian, $\mathbf{A}^{\mathrm{CC2}}(T_1,T_2)$, the ground state cluster amplitudes by those from first-order Møller−Plesset perturbation theory (MP1). This substitution leads to the CIS(D_∞) model[36] for excitation energies. If the Jacobian is in addition symmetrized, one arrives at the ADC(2) secular matrix:[22]

DOI: 10.1021/acs.jctc.8b00396
J. Chem. Theory Comput. 2018, 14, 4640−4650

$$\mathbf{A}^{\mathrm{ADC}(2)} = \frac{1}{2}(\mathbf{A}^{\mathrm{CC2}}(0, T_2^{(\mathrm{MP1})}) + \mathbf{A}^{\mathrm{CC2}}(0, T_2^{(\mathrm{MP1})})^{\dagger}) \tag{18}$$

The PE-ADC(2) secular matrix can be obtained in the same way from the PERI-CC2 Jacobian,[9]

$$\mathbf{A}^{\mathrm{PE-CC2}}_{\mu_i\nu_j} = \begin{pmatrix} \langle\mu_1|\hat{F}^{\mathrm{PE}} + \hat{\tilde{W}}^{\mathrm{QM}} + \hat{\tilde{G}}^{\Delta} + [\hat{\tilde{W}}^{\mathrm{QM}}, \hat{T}_2], \tau_{\nu_1}] + \hat{\tilde{G}}^{\nu_1}|\mathrm{HF}\rangle & \langle\mu_1|[\hat{\tilde{W}}^{\mathrm{QM}}, \tau_{\nu_2}]|\mathrm{HF}\rangle \\ \langle\mu_2|[\hat{\tilde{W}}^{\mathrm{QM}}, \tau_{\nu_1}]|\mathrm{HF}\rangle & \langle\mu_2|[\hat{F}^{\mathrm{PE}}, \tau_{\nu_2}]|\mathrm{HF}\rangle \end{pmatrix} \tag{19}$$

In the last equation, we used T_1-transformed operators defined as $\hat{\tilde{O}} = \exp(-\hat{T}_1)\hat{O}\exp(\hat{T}_1)$ and the derivative of the correlation contribution to the reaction field operator proposed in ref 9 as

$$\hat{G}^{\nu 1} = \frac{\partial \hat{G}^{\Delta}}{\partial t_{\nu_1}} = \sum_{uv}\sum_{pq} \varepsilon^{u}_{pq}\langle \mathrm{HF} + \bar{t}_1|[\hat{E}_{pq}, \tau_{\nu 1}]|\mathrm{HF}\rangle R_{uv} \times \sum_{pq} \varepsilon^{v}_{rs}\hat{E}_{rs} \tag{20}$$

For PE-CC2, the operator $\hat{G}^{\Delta}$ is computed only from the density contribution that originates from the singles cluster amplitudes and singles (ground state) Lagrange multipliers:[9]

$$\hat{G}^{\Delta} = -\sum_{uv} F^{\mathrm{elec}}_{v}(\mathbf{D}^{\Delta})R_{vu}\sum_{pq}\varepsilon^{u}_{pq}\hat{E}_{pq} = \sum_{u}\mu^{\Delta}_{u}\sum_{pq}\varepsilon^{u}_{pq}\hat{E}_{pq} \tag{21}$$

with

$$D^{\Delta}_{pq} = \langle \mathrm{HF} + \bar{t}_1|e^{-\hat{T}_1}\hat{E}_{pq}e^{\hat{T}_1}|\mathrm{HF}\rangle - \langle \mathrm{HF}|\hat{E}_{pq}|\mathrm{HF}\rangle \tag{22}$$

The secular matrix for PE-ADC(2) can be obtained from the PE-CC2 Jacobian in the same way as the vacuum ADC(2) secular matrix from the vacuum CC2 Jacobian. For an easier discussion, we split the PE-ADC(2) secular matrix into a vacuum-like and an embedding contribution, $\mathbf{A}^{\mathrm{PE-ADC}(2)} = \mathbf{A}^{\mathrm{ADC}(2),\mathrm{QM}} + \mathbf{A}^{\mathrm{ADC}(2),\mathrm{PE}}$. Regarding the above approximation for the reaction field, the polarizable embedding contributes only to the singles−singles and the doubles−doubles blocks:

$$A^{\mathrm{ADC}(2),\mathrm{PE}}_{\mu_1,\nu_1} = \langle\mu_1|[\hat{G}^{\mathrm{HF}}, \tau_{\nu_1}] + \hat{G}^{\nu_1}|\mathrm{HF}\rangle \tag{23}$$

$$A^{\mathrm{ADC}(2),\mathrm{PE}}_{\mu_2,\nu_2} = \langle\mu_2|[\hat{G}^{\mathrm{HF}}, \tau_{\nu_2}]|\mathrm{HF}\rangle \tag{24}$$

Note that for ADC(2) the density contribution $\mathbf{D}^{\Delta}$ vanishes since the ground state singles amplitudes and Lagrange multipliers vanish. $\hat{G}^{\mathrm{HF}}$ is included through the Fock matrix $\hat{F}^{\mathrm{PE}}$. Its contributions are already present in the PTE reaction field scheme. The excitonic coupling term[37] that arises from $\hat{G}^{\nu_1}$ originates from the derivative of $\hat{G}^{\Delta}$ with respect to t_{ν_1}, compare eq 20, which are nonvanishing. Its contribution to the linear transformations with the secular matrix during the iterative solution of the eigenvalue equations is implemented via two auxiliary densities:[9]

$$\mathbf{D}^{\eta} = \sum_{\nu_1}\frac{\partial \mathbf{D}^{\Delta}}{\partial t_{\nu_1}}E^{f}_{\nu_1} \quad \text{and} \quad \mathbf{D}^{\xi} = \sum_{\mu_1} E^{f}_{\mu_1}\frac{\partial \mathbf{D}^{\Delta}}{\partial \bar{t}_{\mu_1}} \tag{25}$$

With these densities, the contributions from $\hat{G}^{\nu_1}$ to the contractions of the CC2 Jacobian or the ADC(2) secular matrix with a vector from the right or the left can be evaluated as

$$\sum_{\nu_1}\langle\mu_1|\hat{G}^{\nu_1}|\mathrm{HF}\rangle E^{f}_{\nu_1} = \langle\mu_1|\hat{G}(\mathbf{D}^{\eta})|\mathrm{HF}\rangle \tag{26}$$

$$\sum_{\mu_1} E^{f}_{\mu_1}\langle\mu_1|\hat{G}^{\nu_1}|\mathrm{HF}\rangle = \langle\mathrm{HF}|[\hat{G}(\mathbf{D}^{\xi}), \tau_{\mu_1}]|\mathrm{HF}\rangle \tag{27}$$

Considering that in ADC(2) theory the correlation effects are included up to second-order in the fluctuation potential, using the first-order Møller−Plesset ground state wave function parameters, the canonical choice[22] for defining excited state total energies is to augment the excitation energies with the ground state energy from second-order Møller−Plesset perturbation theory. We use the corresponding approach for PE-ADC(2) and define the total energies of excited states as the sum of the PE-MP2 ground state and the PE-ADC(2) excitation energies. This leads to the following Lagrange function for the total energy of an excited state f:

$$\begin{aligned} L^{\mathrm{PE-ADC}(2),f} = {} & \langle\mathrm{HF}|\hat{F}^{\mathrm{QM}} + \hat{G}^{\mathrm{es}} + \hat{W}^{\mathrm{QM}} + [\hat{W}^{\mathrm{QM}}, \hat{T}_2]|\mathrm{HF}\rangle \\ & + \sum_{i,j=1}^{2}\sum_{\mu_i\nu_j} E^{f}_{\mu_i}A^{\mathrm{PE-ADC}(2)}_{\mu_i\nu_j}E^{f}_{\nu_j} \\ & + \bar{\omega}^{f}\left(1 - \sum_{i=1}^{2}\sum_{\mu_i} E^{f}_{\mu_i}E^{f}_{\mu_i}\right) \\ & + \sum_{\mu_2}\bar{t}^{f}_{\mu_2}\langle\mu_2|[\hat{F}^{\mathrm{PE}}, \hat{T}_2] + \hat{W}^{\mathrm{QM}}|\mathrm{HF}\rangle \\ & + \langle\mathrm{HF}|[\hat{H}^{\mathrm{QM}} + \hat{G}^{\mathrm{HF}}, \hat{\bar{\kappa}}]|\mathrm{HF}\rangle \\ & - \frac{1}{2}\sum_{uv}(F^{\mathrm{ne}}_{u} + F^{\mathrm{elec}}_{u}(\mathbf{D}^{\mathrm{HF}})) \\ & \times R_{uv}(F^{\mathrm{ne}}_{v} + F^{\mathrm{elec}}_{v}(\mathbf{D}^{\mathrm{HF}})) + E^{\mathrm{ne}} \end{aligned} \tag{28}$$

The first term represents the vacuum-like contributions to the PE-MP2 ground state energy plus the interaction of the electron with the static moments at the Hartree−Fock level. The PE-ADC(2) excitation energies are accounted for by the second term where the right and left eigenvectors (E^{f}) are identical since the PE-ADC(2) secular matrix is Hermitian. The third term implements the orthonormality condition for the eigenvectors, and the fourth and fifth terms account for the MP1 amplitude and the Hartree−Fock equations, similar to that in the PE-MP2 Lagrangian. Finally, the last two terms account again for the Hartree−Fock polarization energy and the nonelectronic energy contributions.

Requiring the above Lagrangian to be stationary with respect to the variations of the doubles amplitudes leads to the equations for the Lagrange multipliers $\bar{t}^{f}_{\mu_2}$:

$$\begin{aligned} \frac{\mathrm{d}L^{\mathrm{PE-ADC}(2),f}}{\mathrm{d}t^{f}_{\mu_2}} = {} & \langle\mathrm{HF}|[\hat{W}^{\mathrm{QM}}, \tau_{\mu_2}]|\mathrm{HF}\rangle \\ & + \langle E_1|[[\hat{W}^{\mathrm{QM}}, E_1], \tau_{\mu_2}]|\mathrm{HF}\rangle + \langle\bar{t}^{f}_{2}|[\hat{F}^{\mathrm{PE}}, \tau_{\mu_2}]|\mathrm{HF}\rangle = 0 \end{aligned} \tag{29}$$

As at the MP2 level, the Lagrange multiplier equations contain only PTE-like embedding contributions, which are automatically included by using the Fock matrix and the orbitals from a PE-HF calculation. With canonical MOs, that is, if F^{PE}_{pq} is

DOI: 10.1021/acs.jctc.8b00396
J. Chem. Theory Comput. 2018, 14, 4640−4650

diagonal, the above equations decouple and can be directly inverted, which is important for the efficiency of the ADC(2) implementation.[22] The reaction field scheme with the approximate coupling densities that we use here conserves this important feature of ADC(2).

Requiring the excited state Lagrangian to be stationary with respect to orbital variations gives the CPHF equations that determine the Lagrange multipliers $\bar{\kappa}_{pq}$:

$$\sum_{rs} (\langle \mathrm{HF}|[[\hat{F}^{\mathrm{PE}}, \hat{E}^{-}_{pq}], \hat{E}^{-}_{rs}]|\mathrm{HF}\rangle + A^{\kappa}_{pq,rs})\bar{\kappa}_{rs} = -\eta^{\kappa,\mathrm{PE\text{-}ADC(2)}}_{pq} \tag{30}$$

For easier discussion, we split the right-hand-side vector as $\eta^{\kappa,\mathrm{PE\text{-}ADC(2)}}_{pq} = \eta^{\kappa,\mathrm{PTE\text{-}ADC(2)}}_{pq} + \eta^{\kappa,\mathrm{pol}}_{pq}$ into a PTE part, $\eta^{\kappa,\mathrm{PTE\text{-}ADC(2)}}_{pq}$, which is computed as in the vacuum case but with the MOs and the Fock matrix replaced by their PE counterparts, and the polarization contributions that arise from the excitonic coupling term:

$$\eta^{\kappa,\mathrm{pol}}_{pq} = 2\sum_{t} [G_{pt}(\mathbf{D}^{\eta})(\mathbf{D}^{\xi}_{tq} + \mathbf{D}^{\xi}_{qt}) - G_{qt}(\mathbf{D}^{\eta}) \times (\mathbf{D}^{\xi}_{tp} + \mathbf{D}^{\xi}_{pt})] \tag{31}$$

Once the CPHF equations are solved, the PE-ADC(2) gradients can be calculated as

$$\left(\frac{\mathrm{d}L^{\mathrm{PE\text{-}ADC(2)},f}}{\mathrm{d}x}\right)_{x=0} = \sum_{\alpha\beta} D^{\mathrm{eff,ao}}_{\alpha\beta} h^{[x]}_{\alpha\beta} + \frac{1}{2}\sum_{\alpha\beta\gamma\delta} d^{\mathrm{sep,ao}}_{\alpha\beta\gamma\delta}(\alpha\beta|\gamma\delta)^{[x]} - \sum_{\alpha\beta} F^{\mathrm{eff,ao}}_{\alpha\beta} S^{[x]}_{\alpha\beta} + \sum_{\alpha\beta P} \Delta^{\mathrm{ao},P}_{\alpha\beta}(\alpha\beta|P)^{[x]} - \sum_{PQ} \gamma_{PQ}(P|Q)^{[x]} + \frac{\mathrm{d}\Delta L^{\mathrm{PE},f}}{\mathrm{d}x} \tag{32}$$

In the above equation, $D^{\mathrm{eff,ao}}_{\alpha\beta}$ is the relaxed one-electron density in the atomic orbital (AO) basis where $d^{\mathrm{sep,ao}}_{\alpha\beta\gamma\delta}$ and $F^{\mathrm{eff,ao}}_{\alpha\beta}$ are, respectively, the separable part of the two-electron density and the effective Fock matrix in the AO basis. In eq 32, the fourth and fifth terms originate from the RI approximation. For detailed expressions of the auxiliary three- and two-index densities and integrals, we refer to ref 33. The explicit PE contributions have been collected in the last term, where

$$\Delta L^{\mathrm{PE},f} = -\frac{1}{2}\sum_{uv} (F^{\mathrm{ne}}_{u} + 2F^{\mathrm{elec}}_{u}(\mathbf{D}^{\mathrm{eff}}) - F^{\mathrm{elec}}_{u}(\mathbf{D}^{\mathrm{HF}})) \times R_{uv}(F^{\mathrm{ne}}_{v} + F^{\mathrm{elec}}_{v}(\mathbf{D}^{\mathrm{HF}})) - \sum_{uv} F_{u}(\mathbf{D}^{\xi})R_{uv}F_{v}(\mathbf{D}^{\eta}) + \sum_{pq} D^{\mathrm{eff}}_{pq}\sum_{u} Q^{\mathrm{es}}_{u}\varepsilon^{u}_{pq} + E^{\mathrm{ne}} \tag{33}$$

Differentiation of the PE contribution with respect to a nuclear coordinate x leads to

$$\frac{\mathrm{d}\Delta L^{\mathrm{PE},f}}{\mathrm{d}x} = \sum_{pq} D^{\mathrm{eff}}_{pq}\sum_{u} Q^{\mathrm{HF}}_{u}\frac{\mathrm{d}\varepsilon^{u}_{pq}}{\mathrm{d}x} + \sum_{pq} D^{\mathrm{HF}}_{pq} \times \sum_{u} (Q^{\mathrm{eff}}_{u} - Q^{\mathrm{HF}}_{u})\frac{\mathrm{d}\varepsilon^{u}_{pq}}{\mathrm{d}x} + \sum_{u} Q^{\mathrm{eff}}_{u}\frac{\mathrm{d}\varepsilon^{u}_{\mathrm{nuc}}}{\mathrm{d}x} + \frac{\mathrm{d}E^{\mathrm{LJ}}}{\mathrm{d}x} + \sum_{pq} D^{\eta}_{pq}\sum_{u} Q^{\xi}_{u}\frac{\mathrm{d}\varepsilon^{u}_{pq}}{\mathrm{d}x} + \sum_{pq} D^{\xi}_{pq}\sum_{u} Q^{\eta}_{u}\frac{\mathrm{d}\varepsilon^{u}_{pq}}{\mathrm{d}x} \tag{34}$$

The last two terms arise from the excitonic coupling contribution, which goes beyond the PTE approximation. In these terms, Q^{ξ}_{u} and Q^{η}_{u} are the induced multipole moments calculated with, respectively, the densities $\mathbf{D}^{\xi}$ and $\mathbf{D}^{\eta}$ without including nonelectronic terms (compare eq 21). For ADC(2), these two terms are equivalent so that only one of them needs to be evaluated if it is multiplied by a factor of 2. The first four terms have the same form as for PE-MP2 but are now calculated with the effective density for PE-ADC(2).

The PE-ADC(2) model has been implemented for excitation energies and excited state orbital-relaxed first-order properties and molecular gradients in the development version of the `ricc2` program of the TURBOMOLE package.[29,38]

FIRST APPLICATIONS TO SUPRAMOLECULAR CHEMISTRY

To demonstrate the performance of the PE-ADC(2) model for excited state potential energy surfaces, we have selected two test cases from supramolecular chemistry where it was still possible to do full supermolecular reference calculations. The two test cases are the host−guest complexes of 4-(dimethylamino)benzonitrile, DMABN, and 2,3-diazabicyclo-[2.2.2]oct-2-ene, DBO (see Figure 1), inside cucurbit[7]uril,

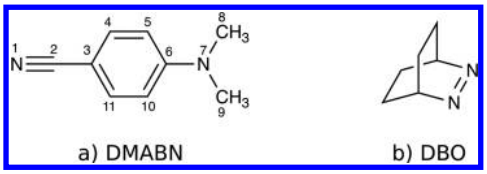


Figure 1. Lewis structures of the guest molecules.

CB[7], as the host molecule, which have interesting photophysical properties.[39−41] The DMABN molecule is a prototype case for a solvent-dependent dual fluorescence that results from emissions from two different electronically excited states: one with a locally excited (LE) character and the other one with an intramolecular charge transfer (ICT) character. The simplicity of its molecular structure as a typical push−pull chromophore made it a subject for many theoretical and experimental studies over the last decades.[42−46] Recently, the UV-vis and fluorescence emission spectra of a DMABN·CB[7] complex in aqueous solution have been studied. They show one absorption and two emission peaks.[41] In contrast to DMABN, DBO has a long but also solvent dependent fluorescence lifetime (up to 1 μs).[39] DBO has been used as a fluorescent probe to measure the polarizability of the inner cavity of CB[7], which is different from solvents.[47]

In addition to the above-mentioned photophysical properties, these host−guest systems have some other helpful

DOI: 10.1021/acs.jctc.8b00396
J. Chem. Theory Comput. 2018, 14, 4640−4650

Table 1. Representative Intramolecular Geometrical Parameters of DMABN in the Ground and the S_1(LE) Excited States from PE-MP2 and PE-ADC(2) in Comparison with the Results from Supermolecular (SM) and Vacuum (vac) Calculations[a]

	ground state			locally excited state		
Internal coord.	SM	PE	vacuum	SM	PE	vacuum
			Selected Torsion Angles (deg)			
$C_8-N_7-C_6-C_{10}$	20.5	20.0	16.2	28.2	15.4	20.3
			Selected Bond Lengths (pm)			
C_3-C_4	141.3	140.8	141.0	140.4	141.0	142.2
C_3-C_{11}	141.2	140.7	141.0	144.8	144.4	142.0
C_4-C_5	140.1	139.8	139.8	142.5	141.3	145.2
$C_{10}-C_{11}$	139.9	139.3	139.8	147.7	146.0	144.9
C_5-C_6	141.6	142.0	142.1	143.3	144.7	142.0
C_6-C_{10}	142.4	141.6	142.1	139.1	140.7	142.5
C_6-N_7	138.6	140.2	139.2	143.6	138.9	140.0
			Selected Out-of-Plane Angles (deg)			
$C_{11}-C_{10}-C_3-H$	1.0	0.0	0.2	−13.1	−10.1	−0.7
$C_6-C_5-N_{10}-C_7$	0.2	−0.2	−0.3	−1.2	−1.2	0.1
			Selected Bond Angles (deg)			
$C_8-N_7-C_9$	115.0	113.4	116.0	116.3	114.9	115.8
$C_2-C_3-C_6$	175.8	178.8	179.9	167.6	170.4	179.9
$N_7-C_6-C_3$	178.4	178.6	178.2	170.7	172.4	179.9
			Intersubsystem Coordinates			
COM displacement (pm)		11			35	
tilting (deg)		2.3			1.0	

[a]The tilting angle is calculated as the angle between the normal vectors of the planes that include the positions of the carbon atoms C_3, C_5, and C_{10} (compare Figure 1).

properties for testing the performance of PE-MP2 and PE-ADC(2) for potential energy surfaces: the host system has only one structural isomer with a relatively rigid structure. Thus, the implemented gradients for PE-MP2 and PE-ADC(2) can be used to optimize the geometries of the guest molecules while keeping the geometry of the host molecule frozen. This excludes evaluation of the results uncertainties from the force field parametrization for the host structure and the effect of temperature fluctuations, which are beyond the scope of the current work. We should emphasize that in other applications these effects may play an important role.

Computational Details: Full Supermolecular Calculations. In the supermolecular MP2 geometry optimization,[33] the structure of the whole DMABN·CB[7] complex was fully optimized. These calculations are done with the cc-pVDZ basis set[48] and the corresponding optimized auxiliary basis set.[49] In the correlated calculations, the frozen core approximation was used for all electrons in 1s orbitals of non-hydrogen atoms. These calculations were carried out with the OMP/MPI parallel RI-MP2 program[34] of the TURBOMOLE package,[29,38] version 7.2, on 8 computer nodes, each with two Intel Xeon E5-2670 CPUs (in total 16 cores) and 64 GB RAM. Under these conditions, one cycle of the MP2 geometry optimization takes about 113 min wall time. Then the full supermolecular QM geometry optimizations for the excited state with local excitation (LE) character of the DMABN·CB[7] complex at the ADC(2)/cc-pVDZ level were done with the OMP/MPI-parallel version of the `ricc2` module of TURBOMOLE on 3 nodes, each with two Intel Xeon E5-2640 CPUs with totally 20 cores and 256 GB memory. These calculations took approximately 10 h per cycle of the geometry optimization. The starting structure for the supermolecular ADC(2) geometry optimization was constructed by positioning the gas phase S_1(LE) structure of DMABN optimized at the ADC(2)/cc-pVDZ level at the center of the CB[7] cavity. The supermolecular ADC(2) geometry optimization required from this starting structure more than 70 steps to converge to a geometry with a Cartesian gradient norm of 0.00018 and with the changes of the total energy smaller than 10^{-6} au.

Computational Details: PE-QM Calculations. For the PE calculations, one needs in addition to the coordinates for QM and MM systems static distributed multipole moments and dipole−dipole polarizabilities for the MM system and, for geometry optimizations, also Lennard-Jones parameters for the interaction between the MM and the QM atoms. For our calculations, we used the atomic charges and dipole and quadrupole moments from an intrinsic atomic orbital[50] (IAO) analysis of the electron density from a DFT/B3LYP-D3(bj) calculation[51−53] on the host structure in the cc-pVDZ basis set for the corresponding host geometry of each PE calculation, *vide infra*. The isotropic polarizabilities were determined as proposed in ref 54, and the anisotropic dipole polarizabilities are set to zero. Finally, the Lennard-Jones parameters for the atoms of the host molecule were taken from ref 55, and the parameters of the guest molecules, DMABN and DBO, were taken from refs 56 and 57, respectively, if an atom type was not defined in ref 55.

Also the PE-MP2 and PE-ADC(2) calculations used the RI and the frozen core approximations. All electrons in the 1s orbitals of non-hydrogen atoms were excluded from the MP2 and ADC(2) calculations. Again, the cc-pVDZ orbital and auxiliary basis sets were used for the geometry optimizations to allow a direct comparison with the supermolecular calculations. A typical PE-MP2 step for one cycle of the geometry optimization of the DMABN·CB[7] complex was finished on one node with Intel Xeon X5670 CPUs (in total 12 cores with 42 GB RAM) after 24 s, and the calculation on the excited state with PE-ADC(2) took 113 s on the same machine. The vacuum MP2/cc-pVDZ and ADC(2)/cc-pVDZ calculations for the DMABN molecule took 18 and 108 s, respectively, on

DOI: 10.1021/acs.jctc.8b00396
J. Chem. Theory Comput. 2018, 14, 4640−4650

the same machine. Therefore, one can conclude that the computational cost of PE-ADC(2) and PE-MP2 calculations are close to the computational cost of vacuum calculations where the environmental effects are completely neglected.

Geometry Optimizations with PE-MP2 and PE-ADC(2). To study the error in the geometries that is introduced by describing the host−guest interaction within the PE approximations, we started for the DMABN molecule from the structures obtained in the full supermolecular MP2 and ADC(2) calculations, kept the coordinates for the CB[7] host frozen, and reoptimized the coordinates of the guest with PE-MP2 and PE-ADC(2). To check if the host molecule has a significant impact on the intramolecular geometry of DMABN, we compare in addition with results from vacuum MP2 and ADC(2) calculations. The results are summarized in Table 1. A comparison between the optimized ground state geometries from PE-MP2 and supermolecular MP2 is shown in Figure 2.

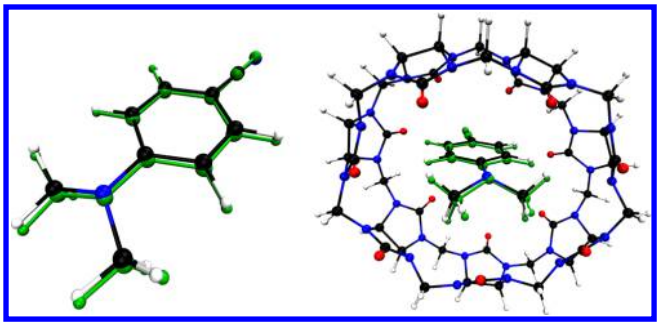


Figure 2. Comparison of the intra- and inter-subsystem coordinates from PE-MP2 and supermolecular MP2 for the ground state of DMABN·CB[7]. (left) Supermolecular MP2 structure (atom colors) superimposed on the PE-MP2 structure of DMABN (green). The host molecule is not shown for clarity. (right) Supermolecular MP2 geometry (atom colors) for the complex superimposed on the structure from PE-MP2 (green).

Both the intermolecular (between the host and guest system) and the intramolecular coordinates of the guest molecule (DMABN) are in good agreement. The mean absolute deviations are 0.36 pm for the bond lengths and 0.26° for the bond angles in the DMABN guest molecule, but in general the influence of the host on the internal coordinates of DMABN is small in the ground state. The DMABN center-of-mass for the PE-MP2 ground state structure is shifted by 11 pm and the molecular plane is tilted by ∼2°, comparing to the supermolecular MP2 structure. Compared with the intermolecular distances in the DMABN·CB[7] complex, this is a relatively small displacement, as can be seen in Figure 2.

The host effects are stronger in the excited state. In Figure 3, the fully optimized structure of DMABN·CB[7] for the S_1(LE) minimum at the ADC(2)/cc-pVDZ level is compared with the structure obtained with PE-ADC(2)/cc-pVDZ with a frozen host structure. In vacuum, the benzene ring in the S_1(LE) minimum exhibits a prominent antiquinoidal distortion. The interaction with the CB[7] host leads to a rotation of the nodes in the virtual natural transition orbital (NTO) shown in Table 2. As a consequence, the benzene ring shows a markedly different bond length distortion: the C_3-C_{11}, $C_{10}-C_{11}$, and C_5-C_6 bonds are 1−3 pm longer and the C_3-C_4, C_4-C_5, and C_6-C_{11} bonds are 1−4 pm shorter than those in the vacuum structure. This distortion is qualitatively correct in the PE-ADC(2) calculation, although not quantitatively reproduced.

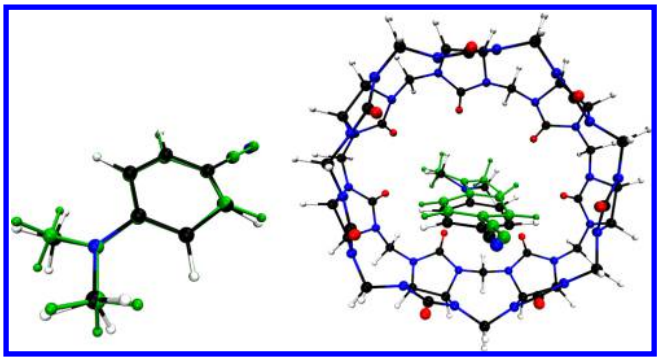


Figure 3. Comparison of the intra- and inter-subsystem coordinates from PE-ADC(2) and supermolecular ADC(2) for the S_1(LE) minimum of DMABN·CB[7]. (left) Supermolecular ADC(2) structure (atom colors) superimposed on the PE-ADC(2) structure of DMABN (green). The host molecule is not shown for clarity. (right) Supermolecular MP2 geometry (atom colors) for the complex superimposed on the structure from PE-MP2 (green).

Also the changes in the bending angles of the −CN and $-N(CH_3)_2$ functional groups, the $C_2-C_3-C_6$ and $N_7-C_6-C_3$ angles, respectively, are qualitatively reproduced by the PE-ADC(2) model (see Table 1). The mean absolute deviation in the intramolecular bond lengths at 0.75 pm is about a factor of 2 larger than that in the ground state. Also the shift of the center of mass of DMABN between the supermolecular and the PE calculation for the S_1(LE) minimum is two times larger than that for the ground state. But these deviations are still small considering that the Lennard-Jones parameters have not been optimized for the PE-MP2 and PE-ADC(2) calculations. The main reason for the larger errors in the S_1(LE) state is probably that the binding energy is significantly higher than in the ground state. The supermolecular calculation gives a binding energy of 143 kJ·mol^{-1} for the ground state at the MP2/cc-pVDZ level and 200 kJ·mol^{-1} for the S_1(LE) state at the ADC(2)/cc-pVDZ level (in both cases not counterpoise corrected). One should also be aware that the supermolecular calculation has a larger basis set superposition error for the excited state than for the ground state because the populated virtual NTO is more diffuse than the depopulated occupied NTO. The PE-MP2 and PE-ADC(2) calculations, however, do not suffer from basis set superposition errors for the host−guest interaction.

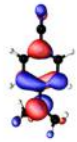
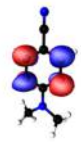
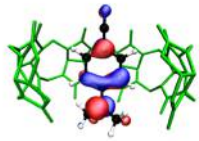
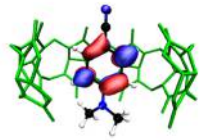
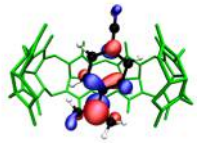
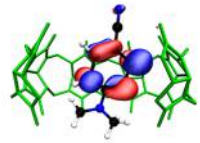
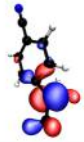
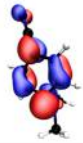
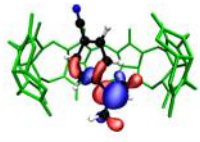
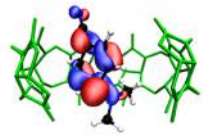
Based on the reported timings, it is clear that pursuing supermolecular MP2 or ADC(2) calculations for systems larger than the studied complexes, for example, a chromophore bound to a protein, is not feasible.

Complexation Effect on the Fluorescence Energies. To investigate the effect of the supramolecular complexation on fluorescence energies, we studied two examples, DMABN·CB[7] and DBO·CB[7], and applied a slightly cheaper computational protocol than in the previous section. The structure of the CB[7] host was kept fixed in the MP2/cc-pVDZ ground state geometry for both complexes, while the coordinates of the DMABN and DBO guest molecules were optimized at the PE-ADC(2)/cc-pVDZ level.

For DMABN, we calculated the fluorescence emission energies out of the two minima of the lowest excited singlet state, S_1(LE) and S_1(ICT). The fluorescence energies of the LE and the twisted ICT states of DMABN·CB[7] complex have been measured experimentally in aqueous solutions.[41] The experimental fluorescence energy for the LE state is 3.50

DOI: 10.1021/acs.jctc.8b00396
J. Chem. Theory Comput. 2018, 14, 4640−4650

Table 2. Character of Lowest Electronic Excitation and Its Molecular Environment, Occupied (occ) and Virtual (vir) Natural Transition Orbitals, and Relative Contribution of the NTO Pair in the Excitations[a]

	occ.	vir.	Contrib.
LE vacuum			92.7%
LE CB7			95.5%
LE SM			98.0%
ICT vacuum			99.8%
ICT CB7			99.6%

[a]The isosurface values for the visualization were set to ±0.05 for all NTOs.

eV, which is in a very good agreement with the PE-ADC(2) result of 3.68 eV. The PE-ADC(2) result for the fluorescence energy of 2.05 eV for the twisted ICT state is 0.45 eV below the band maximum in the experimental fluorescence spectrum at 2.5 eV. This is in line with the CC2 results for the vacuum case from ref 44, which also is ∼0.3−0.7 eV below the experimental band maxima in nonpolar solvents.

As another example we studied the nπ^* transition of DBO in the supramolecular complex with CB[7]. For this case, we also investigated the basis set dependence of the vertical excitation and fluorescence energy with different basis sets, see Table 3. The vertical excitation and fluorescence energies show a stable convergence for the cc-pVXZ (X= D, T, Q) basis sets, but they both collapse when diffuse functions are added as in the aug-cc-pVDZ basis. This issue is known in the literature as the charge penetration error or electrostatic catastrophe and occurs when the electron density of the QM region leaks significantly out into the MM region.[17,58,59]

The natural transition orbitals for the DBO·CB[7] complex calculated at the PE-ADC/aug-cc-pVDZ level of theory with different embedding potentials are shown in Table 4. In the vacuum case, the lowest electronic excitation has nπ^* character, and the vertical excitation energy is 3.47 eV, which is in good agreement with the experimental band maximum λ_{max} of the UV-vis spectrum at 3.31 eV.[40] For the cc-pVTZ and cc-pVQZ basis sets also the vacuum to CB[7] shift in the vertical excitation and fluorescence emission energies fit with,

Table 3. Vertical Excitation (VEE) and Fluorescence Emission Energies (FEE) of DBO·CB[7] Calculated at (ECP)/PE-ADC(2) with Different Basis Sets[a]

	gas phase		inside CB[7]		inside CB[7] (ECP)	
basis	VEE	FEE	VEE	FEE	VEE	FEE
cc-pVDZ	3.54	2.72	3.55	2.74	3.55	2.74
cc-pVTZ	3.46	2.65	3.47	2.67	3.47	2.67
cc-pVQZ	3.43	2.62	3.44	2.65	3.44	2.65
aug-cc-pVDZ	3.47	2.65	0.64	0.20	3.48	2.67
d-aug-cc-pVDZ	3.47	2.64	n.c.	n.c.	3.48	2.67
exptl[b]	3.31	2.79	3.32	2.82	3.32	2.82

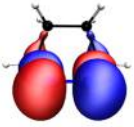
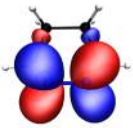
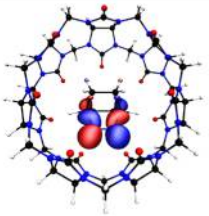
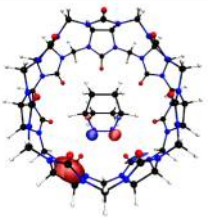
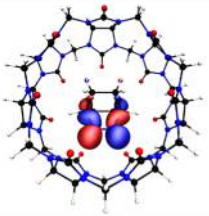
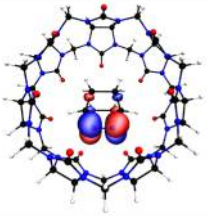
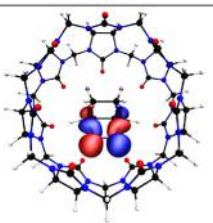
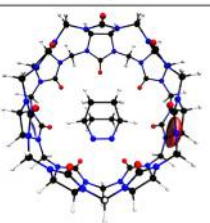
[a]All VEEs and FEEs are calculated at PE-MP2/cc-pVDZ and PE-ADC(2)/cc-pVDZ optimized geometries. See the text for further details. [b]Measured in an aqueous solution, ref 40.

respectively, −0.01 and +0.03 eV to the experimental results reported in ref 40.

However, in the PE-ADC(2) calculations with the aug-cc-pVDZ basis set, the excitation and fluorescence energies collapse to unphysical low values. The virtual natural transition orbital shown in Table 4 is in this case an orbital that is localized in the host structure and only accessible for the excitation process because the embedding potential does not account for the Pauli repulsion by the hosts electrons. We have analyzed this problem in more detail to identify to which components of the electrostatic embedding (static charges,

DOI: 10.1021/acs.jctc.8b00396
J. Chem. Theory Comput. 2018, 14, 4640−4650

Table 4. Environment Potential Used in the Calculation, Vertical Excitation Energies (VEE, given in eV) Calculated at PE-ADC(2)/aug-cc-pVDZ Level, Occupied (occ) and Virtual (vir) Natural Transition Orbitals, and Their Contributions to the Eigenvector

Potential	VEE	occ.	vir.	Contrib.
vacuum	3.47			99.8%
charges dipoles quadrupoles polarizability	0.64			99.4%
charges dipoles polarizability	3.55			99.7%
quadrupoles	0.85			99.9%

dipoles, quadrupoles or induced dipoles, that is, polarizabilities) the excitation energies are most sensitive. It turned out that in this case the vertical excitation energy collapses only when the static quadrupoles are included in the embedding potential (see Table 4). The expected nπ^* transition is recovered if we exclude quadrupoles from the embedding potential. The importance of the quadrupole moments for accurate embedding potentials has been discussed before in the context of various electrostatic models.[60−63] In agreement with earlier observations, the exclusion of the quadrupoles has a significant effect on the excitation energies. Excluding quadruples in DBO·CB[7] shifts up the S_1 vertical excitation energy by 0.1 eV. To address this problem appropriately a robust embedding method must account somehow for the Pauli repulsion interaction. In this regard, we carried out pilot calculations where we added effective core potentials (ECP) to each non-hydrogen MM site to mimic at least partially the Pauli repulsion. In this test, we used the full PE potential (partial charges, dipoles, quadrupoles, and dipole polarizabilities) and, because pseudopotentials optimized for this purpose are not yet available, relativistic 2 electron SEFIT ECPs[64] for the MM subsystem. The results for VEEs and FEEs are presented in Table 3. With adding the nonelectrostatic contributions of the pseudopotentials, the charge leaking issue can be avoided and the VEE and FEE can be calculated with the same accuracy for the diffuse basis sets as for the other basis sets. Moreover the results of the ECP/PE embedding model are very close to those from the PE embedding model without pseudopotentails for the basis sets without diffuse functions, which indicates that there are no artificial effects from the ECPs.

CONCLUSION

Analytic molecular gradients have been implemented for ground states at the PE-MP2 and for excited states at the PE-ADC(2) level into the `ricc2` program of the development version of the TURBOMOLE package.[38] In this implementation, the post-HF contributions to the reaction field potential is included in the ADC(2) response calculations via an approximate coupling density, which is calculated only from the single excitation parts of the excited state eigenvectors. This approach was used before successfully for the coupled cluster model CC2 and has the advantage that it conserves the high efficiency of the RI-CC2 or RI-ADC(2) implementations.[9]

The performance of the geometry optimizations with the QM/MM PE-ADC(2) gradients has been validated by a comparison to supermolecular MP2 and ADC(2) calculations for the DMABN·CB[7] host−guest complex. The QM/MM geometries can reproduce both the internal coordinates of the QM subsystem and its position and orientation in its environment reasonably provided that the interaction with the environment is small enough so that the assumptions that

DOI: 10.1021/acs.jctc.8b00396
J. Chem. Theory Comput. 2018, 14, 4640−4650

underlie the QM/MM partitioning are valid. The use of basis sets with diffuse functions is problematic, however, if the embedding potential does not include any terms that model the Pauli repulsion, as it is the case for the original PE model that is used here. The diffuse functions enhance the charge leaking problem and can lead to low lying unphysical QM to MM charge transfer excitations, as demonstrated in the example of the DBO·CB[7] complex. Preliminary calculations show that pseudopotentials can be used as a remedy for the latter problem, although to exploit the full potential of this approach, the effective potentials should to be optimized for hydrogens and also the valence electrons of the other atoms. Research in this direction is continued in our lab. The computational costs for PE-ADC(2) gradient calculations are only marginally higher than that for a corresponding gas phase calculation. Because of the low computational costs, PE-MP2 and PE-ADC(2) gradient calculations can be done many times for medium-sized systems (e.g., $\lesssim$50 atoms) and thus be used to study the (short-time) dynamics after photoexcitation or to calculate intrinsic reaction coordinate pathways for relaxation processes at similar computational costs as for isolated systems. If the accuracy of the QM/MM approximation is controlled properly, this method can thus be used to study excited state potential energy surfaces and the short time dynamics after photoexcitation of medium size systems in complex molecular environments.

■ ASSOCIATED CONTENT

Supporting Information

The Supporting Information is available free of charge on the ACS Publications website at DOI: 10.1021/acs.jctc.8b00396.

Detailed information on the obtained reaction and interaction energies for both test sets (PDF)

■ AUTHOR INFORMATION

Corresponding Author

*E-mail: Alireza.MarefatKhah@ruhr-uni-bochum.de.

ORCID

Alireza Marefat Khah: 0000-0002-9593-0344

Christof Hättig: 0000-0002-5752-2710

Notes

The authors declare no competing financial interest.

■ ACKNOWLEDGMENTS

We are grateful to Prof. Jacob Kongsted and Dr. Jógvan Magnus Haugaard Olsen for providing us test cases of their PE-DFT implementation and for useful discussions. Financial support by Deutsche Forschungsgemeinschaft (DFG) through the cluster of excellence RESOLV (EXC 1069) and projects Ha 2588/8-1 and 2588/10-1 is gratefully acknowledged.

■ REFERENCES

(1) Klymchenko, A. S. Solvatochromic and fluorogenic dyes as environment-sensitive probes: design and biological applications. *Acc. Chem. Res.* **2017**, *50*, 366−375.

(2) Warshel, A.; Karplus, M. Calculation of ground and excited state potential surfaces of conjugated molecules. I. Formulation and parametrization. *J. Am. Chem. Soc.* **1972**, *94*, 5612−5625.

(3) Warshel, A.; Levitt, M. Theoretical studies of enzymic reactions: Dielectric, electrostatic and steric stabilization of the carbonium ion in the reaction of lysozyme. *J. Mol. Biol.* **1976**, *103*, 227−249.

(4) Senn, H. M.; Thiel, W. QM/MM Methods for Biomolecular Systems. *Angew. Chem., Int. Ed.* **2009**, *48*, 1198−1229.

(5) Olsen, J. M. H.; Kongsted, J. Molecular properties through polarizable embedding. *Adv. Quantum Chem.* **2011**, *61*, 107−143.

(6) List, N. H.; Olsen, J. M. H.; Kongsted, J. Excited states in large molecular systems through polarizable embedding. *Phys. Chem. Chem. Phys.* **2016**, *18*, 20234−20250.

(7) Olsen, J. M. H.; Aidas, K.; Kongsted, J. Excited States in Solution through Polarizable Embedding. *J. Chem. Theory Comput.* **2010**, *6*, 3721−3734.

(8) Sneskov, K.; Schwabe, T.; Kongsted, J.; Christiansen, O. The polarizable embedding coupled cluster method. *J. Chem. Phys.* **2011**, *134*, 104108.

(9) Schwabe, T.; Sneskov, K.; Haugaard Olsen, J. M.; Kongsted, J.; Christiansen, O.; Hättig, C. PERI-CC2: A Polarizable Embedded RI-CC2 Method. *J. Chem. Theory Comput.* **2012**, *8*, 3274.

(10) List, N. H.; Coriani, S.; Kongsted, J.; Christiansen, O. Lanczos-driven coupled-cluster damped linear response theory for molecules in polarizable environment. *J. Chem. Phys.* **2014**, *141*, 244107.

(11) Hedegård, E. D.; List, N. H.; Jensen, H. J. A.; Kongsted, J. The multi-configuration self-consistent field method within a polarizable embedded framework. *J. Chem. Phys.* **2013**, *139*, 044101.

(12) Hedegård, E. D.; Jensen, H. J. A.; Kongsted, J. Polarizable Embedding Based on Multiconfigurational Methods: Current Developments and the Road Ahead. *Int. J. Quantum Chem.* **2014**, *114*, 1102−1107.

(13) List, N. H.; Beerepoot, M. T. P.; Olsen, J. M. H.; Gao, B.; Ruud, K.; Jensen, H. J. A.; Kongsted, J. Molecular quantum mechanical gradients within the polarizable embedding approach-Application to the internal vibrational Stark shift of acetophenone. *J. Chem. Phys.* **2015**, *142*, 034119.

(14) Caprasecca, S.; Jurinovich, S.; Viani, L.; Curutchet, C.; Mennucci, B. Geometry Optimization in Polarizable QM/MM Models: The Induced Dipole Formulation. *J. Chem. Theory Comput.* **2014**, *10*, 1588−1598.

(15) Li, H. Analytic Energy Gradient in Combined Second-Order Møller-Plesset Perturbation Theory and Polarizable Force Field Calculation. *J. Phys. Chem. A* **2011**, *115*, 11824−11831.

(16) Zeng, Q.; Liang, W. Analytic energy gradient of excited electronic state within TDDFT/MMpol framework: Benchmark tests and parallel implementation. *J. Chem. Phys.* **2015**, *143*, 134104.

(17) Menger, M. F. S. J.; Caprasecca, S.; Mennucci, B. Excited-State Gradients in Polarizable QM/MM Models: An Induced Dipole Formulation. *J. Chem. Theory Comput.* **2017**, *13*, 3778−3786.

(18) Yanai, T.; Tew, D.; Handy, N. C. A new hybrid exchange-correlation functional using the Coulomb-attenuating method (CAM-B3LYP). *Chem. Phys. Lett.* **2004**, *393*, 51−57.

(19) Eriksen, J. J.; Sauer, S. P.; Mikkelsen, K. V.; Christiansen, O.; Jensen, H. J. A.; Kongsted, J. Failures of TDDFT in describing the lowest intramolecular charge-transfer excitation in para-nitroaniline. *Mol. Phys.* **2013**, *111*, 1235−1248.

(20) Christiansen, O.; Koch, H.; Jørgensen, P.; Helgaker, T. The second-order approximate coupled cluster singles and doubles model CC2. *Chem. Phys. Lett.* **1996**, *263*, 530−539.

(21) Schirmer, J. Beyond the random-phase approximation: A new approximation scheme for the polarization propagator. *Phys. Rev. A: At., Mol., Opt. Phys.* **1982**, *26*, 2395.

(22) Hättig, C. Structure optimizations for excited states with correlated second-order methods: CC2 and ADC(2). *Adv. Quantum Chem.* **2005**, *50*, 37.

(23) List, N. H.; Olsen, J. M. H.; Rocha-Rinza, T.; Christiansen, O.; Kongsted, J. Performance of Popular XC-Functionals for the Description of Excitation Energies in GFP-Like Chromophore Models. *Int. J. Quantum Chem.* **2012**, *112*, 789−800.

(24) Jacquemin, D.; Duchemin, I.; Blase, X. 0−0 Energies Using Hybrid Schemes: Benchmarks of TD-DFT, CIS(D), ADC(2), CC2 and BSE/GW formalism for 80 Real-Life Compounds. *J. Chem. Theory Comput.* **2015**, *11*, 5340.

DOI: 10.1021/acs.jctc.8b00396
J. Chem. Theory Comput. 2018, 14, 4640−4650

(25) Winter, N. O.; Graf, N. K.; Leutwyler, S.; Hättig, C. Benchmarks for 0−0 transitions of aromatic organic molecules: DFT/B3LYP, ADC(2), CC2, SOS-CC2 and SCS-CC2 compared to high-resolution gas-phase data. *Phys. Chem. Chem. Phys.* **2013**, *15*, 6623−6630.
(26) Tuna, D.; Lefrancois, D.; Wolański, Ł; Gozem, S.; Schapiro, I.; Andruniów, T.; Dreuw, A.; Olivucci, M. Assessment of Approximate Coupled-Cluster and Algebraic-Diagrammatic-Construction Methods for Ground- and Excited-State Reaction Paths and the Conical-Intersection Seam of a Retinal-Chromophore Model. *J. Chem. Theory Comput.* **2015**, *11*, 5758−5781.
(27) List, N. H.; Norman, P.; Kongsted, J.; Jensen, H. J. A. A quantum-mechanical perspective on linear response theory within polarizable embedding. *J. Chem. Phys.* **2017**, *146*, 234101.
(28) Helgaker, T.; Jørgensen, P.; Olsen, J. *Molecular Electronic-structure Theory*; John Wiley & Sons, Ltd, 2000.
(29) *TURBOMOLE*, V7.2 2017, a development of University of Karlsruhe and Forschungszentrum Karlsruhe GmbH, 1989−2007, TURBOMOLE GmbH, since 2007; available from http://www.turbomole.com.
(30) Hršak, D.; Marefat Khah, A.; Christiansen, O.; Hättig, C. Polarizable Embedded RI-CC2 Method for Two-Photon Absorption Calculations. *J. Chem. Theory Comput.* **2015**, *11*, 3669−3678.
(31) del Valle, F. J. O.; Tomasi, J. Electron correlation and solvation effects. I. Basic formulation and preliminary attempt to include the electron correlation in the quantum mechanical polarizable continuum model so as to study solvation phenomena. *Chem. Phys.* **1991**, *150*, 139−150.
(32) Ángyán, J. G. Choosing between alternative MP2 algorithms in the self-consistent reaction field theory of solvent effects. *Chem. Phys. Lett.* **1995**, *241*, 51−56.
(33) Weigend, F.; Häser, M. RI-MP2: first derivatives and global consistency. *Theor. Chem. Acc.* **1997**, *97*, 331−340.
(34) Hättig, C.; Hellweg, A.; Köhn, A. Distributed memory parallel implementation of energies and gradients for second-order Møller-Plesset perturbation theory with the resolution-of-the-identity approximation. *Phys. Chem. Chem. Phys.* **2006**, *8*, 1159−1169.
(35) Christiansen, O.; Jørgensen, P.; Hättig, C. Response Functions from Fourier Component Variational Perturbation Theory Applied to a Time-Averaged Quasienergy. *Int. J. Quantum Chem.* **1998**, *68*, 1−52.
(36) Head-Gordon, M.; Oumi, M.; Maurice, D. Quasidegenerate second-order perturbation corrections to single-excitation configuration interactionn. *Mol. Phys.* **1999**, *96*, 593−602.
(37) Lunkenheimer, B.; köhn, A. Solvent Effects on Electronically Excited States Using the Conductor-Like Screening Model and the Second-Order Correlated Method ADC(2). *J. Chem. Theory Comput.* **2013**, *9*, 977.
(38) Furche, F.; Ahlrichs, R.; Hättig, C.; Klopper, W.; Sierka, M.; Weigend, F. Turbomole. *WIREs Comput. Mol. Sci.* **2014**, *4*, 91.
(39) Nau, W. M.; Greiner, G.; Rau, H.; Wall, J.; Olivucci, M.; Scaiano, J. C. Fluorescence of 2,3-Diazabicyclo[2.2.2]oct-2-ene Revisited: Solvent-Induced Quenching of the $n\pi^*$ Excited State by an Aborted Hydrogen Atom Transfer. *J. Phys. Chem. A* **1999**, *103*, 1579−1584.
(40) Marquez, C.; Nau, W. M. Polarizabilities Inside Molecular Containers. *Angew. Chem., Int. Ed.* **2001**, *40*, 4387−4390.
(41) Sayed, M.; Biedermann, F.; Uzunova, V. D.; Assaf, K. I.; Bhasikuttan, A. C.; Pal, H.; Nau, W. M.; Mohanty, J. Triple Emission from p-Dimethylaminobenzonitrile-Cucurbit[8]uril Triggers the Elusive Excimer Emission. *Chem. - Eur. J.* **2015**, *21*, 691−696.
(42) Georgieva, I.; Aquino, A. J. A.; Plasser, F.; Trendafilova, N.; Köhn, A.; Lischka, H. Intramolecular Charge-Transfer Excited-State Processes in 4-(N,N-Dimethylamino)benzonitrile: The Role of Twisting and the $\pi\sigma^*$ State. *J. Phys. Chem. A* **2015**, *119*, 6232−6243.
(43) Georgieva, I.; Aquino, A. J. A.; Plasser, F.; Trendafilova, N.; Köhn, A.; Lischka, H. Intramolecular Charge-Transfer Excited-State Processes in 4-(N,N-Dimethylamino)benzonitrile: The Role of Twisting and the $\pi\sigma^*$ State. *J. Phys. Chem. A* **2015**, *119*, 6232−6243.
(44) Köhn, A.; Hättig, C. On the nature of the low-lying singlet states of dmabn. *J. Am. Chem. Soc.* **2004**, *126*, 7399−7410.
(45) Hättig, C.; Hellweg, A.; Köhn, A. Intramolecular charge transfer mechanism in quinolidines: the role of the amino twist angle. *J. Am. Chem. Soc.* **2006**, *128*, 15672−15682.
(46) Curchod, B. F. E.; Sisto, A.; Martínez, T. J. Ab initio multiple spawning photochemical dynamics of DMABN using GPUs. *J. Phys. Chem. A* **2017**, *121*, 265−276.
(47) Assaf, K. I.; Nau, W. M. Curcubiturils: from synthesis to high-affinity binding and catalysis. *Chem. Soc. Rev.* **2015**, *44*, 394−418.
(48) Dunning, T. H. Gaussian basis sets for use in correlated molecular calculations. I. The atoms boron through neon and hydrogen. *J. Chem. Phys.* **1989**, *90*, 1007−1023.
(49) Weigend, F.; Köhn, A.; Hättig, C. Efficient use of the correlation consistent basis sets in resolution of the identity MP2 calculations. *J. Chem. Phys.* **2002**, *116*, 3175−3183.
(50) Knizia, G. Intrinsic Atomic Orbitals: An Unbiased Bridge between Quantum Theory and Chemical Concepts. *J. Chem. Theory Comput.* **2013**, *9*, 4834−4843.
(51) Becke, A. D. Density-functional thermochemistry. III. The role of exact exchange. *J. Chem. Phys.* **1993**, *98*, 5648−5652.
(52) Grimme, S.; Antony, J.; Ehrlich, S.; Krieg, H. A consistent and accurate ab initio parametrization of density functional dispersion correction (DFT-D) for the 94 elements H-Pu. *J. Chem. Phys.* **2010**, *132*, 154104.
(53) Grimme, S.; Ehrlich, S.; Goerigk, L. Effect of the damping function in dispersion corrected density functional theory. *J. Comput. Chem.* **2011**, *32*, 1456.
(54) Schröder, H.; Schwabe, T. Efficient Determination of Accurate Atomic Polarizabilities for Polarizable Embedding Calculations. *J. Comput. Chem.* **2016**, *37*, 2052−2059.
(55) Cornell, W. D.; Cieplak, P.; Bayly, C. I.; Gould, I. R.; Merz, K. M.; Ferguson, D. M.; Spellmeyer, D. C.; Fox, T.; Caldwell, J. W.; Kollman, P. A. A Second Generatio Force Field for the Simulation of Proteins, Nucleic Acids and Organic Molecules. *J. Am. Chem. Soc.* **1995**, *117*, 5179−5197.
(56) Jorgensen, W. L.; Laird, E. R.; Nguyen, T. B.; Tirado-Rives, J. Monte Carlo Simulations of Pure Liquid Substitued Benzenes with OPLS Potential Functions. *J. Comput. Chem.* **1993**, *14*, 206−215.
(57) Schäfer, L. V.; Müller, E. M.; Gaub, H. E.; Grubmüller, H. Elastic Properties of Photoswitchable Azobenzene Polymers from Molecular Dynamics Simulations. *Angew. Chem., Int. Ed.* **2007**, *46*, 2232−2237.
(58) Reinholdt, P.; Olsen, J. M. H.; Kongsted, J. Polarizable Density Embedding: A Solution to the Electron Spill-Out Problem in Multiscale Modeling. *J. Phys. Chem. Lett.* **2017**, *8*, 5949−5958.
(59) Demerdash, O.; Mao, Y.; Liu, T.; Head-Gordon, M.; Head-Gordon, T. Assessing many-body contributions to intermolecular interactions of the AMOEBA force field using energy decomposition analysis of electronic structure calculations. *J. Chem. Phys.* **2017**, *147*, 161721.
(60) Narth, C.; Lagardère, L.; Polack, E.; Gresh, N.; Wang, Q.; Bell, D. R.; Rackers, J. A.; Ponder, J. W.; Ren, P. Y.; Piquemal, J.-P. Scalable Improvement of SPME Multipolar Electrostatics in Anisotropic Polarizable Molecular Mechanics Using a General Short-Range Penetration Correction up to Quadrupoles. *J. Comput. Chem.* **2016**, *37*, 494−505.
(61) Misquitta, A. J.; Stone, A. J. Ab initio Atom-Atom Potentials Using CAMCASP: Theory and Application to Many-Body Models for Pyridine Dimer. *J. Chem. Theory Comput.* **2016**, *12*, 4184−4208.
(62) Rackers, J. A.; Wang, Q.; Liu, C.; Piquemal, J.-P.; Ren, P.; Ponder, J. W. An optimized charge penetration model for use with the AMOEBA force field. *Phys. Chem. Chem. Phys.* **2017**, *19*, 276−291.
(63) Elking, D. M.; Cisneros, G. A.; Piquemal, J.-P.; Darden, T. A.; Pedersen, L. G. Gaussian Multipole Model (GMM). *J. Chem. Theory Comput.* **2010**, *6*, 190−202.
(64) Igel-Mann, G.; Stoll, H.; Preuss, H. Pseudopotentials for main group elements (IIIa through VIIa). *Mol. Phys.* **1988**, *65*, 1321−1328.

DOI: 10.1021/acs.jctc.8b00396
J. Chem. Theory Comput. 2018, 14, 4640−4650